MATERIALS
CHEMISTRY
FRONTIERS

RESEARCH ARTICLE

Check for updates

Single-crystalline CoFe nanoparticles encapsulated in N-doped carbon nanotubes as a bifunctional catalyst for water splitting†

Xiaojun Zeng,[ab] Myeong Je Jang,[cd] Sung Mook Choi, [iD][c] Hyun-Seok Cho,[e] Chang-Hee Kim,[e] Nosang Vincent Myung*[f] and Yadong Yin [iD] *[b]

Single-crystalline CoFe alloy nanoparticles encapsulated in nitrogen-doped carbon nanotubes (CoFe@N–C) were synthesized through a simple heat-treatment in an N_2 environment. CoFe@N–C effectively catalyzed the overall water splitting in alkaline media. Specifically, the as-synthesized CoFe@N–C exhibited excellent activity towards the oxygen evolution reaction (OER) with a low over-potential of 292 mV at 10 mA cm^{-2} and the hydrogen evolution reaction (HER) with a low overpotential of 110 mV at 10 mA cm^{-2}. The good electrocatalytic properties may be attributed to the synergistic electronic coupling between single-crystalline CoFe and highly conductive N-doped CNTs and the enrichment of active sites. Additionally, CoFe@N–C showed excellent stability and durability with no observable deviation in the overpotential for the OER and HER after 1000 cycles of cyclic voltammetry (CV).

Introduction

Electrochemical water splitting is widely regarded as a cost-effective and environmentally friendly technology for the production of hydrogen and oxygen.[1,2] Ideal electrocatalysts are expected to accelerate the sluggish anodic oxygen evolution reaction (OER) and the facile cathodic hydrogen evolution reaction (HER).[3] To date, noble metal-based materials are the state-of-the-art electrocatalysts for water splitting (*e.g.*, Pt for the HER and RuO_2/IrO_2 for the OER) due to their very low overpotentials and excellent reaction kinetics. However, the high cost and scarcity of noble metals, together with the susceptibility of Pt to poisoning, hinder their large-scale application.[4,5] Moreover, these noble metal-based materials can only be used as either HER catalysts or OER catalysts rather than exhibiting bifunctional catalytic activity.[6,7] Thus, it is highly desirable to develop an efficient bifunctional catalyst based on earth-abundant elements for overall water splitting, which however remains a big challenge.[8]

Recently, various low-cost and highly efficient electrocatalysts for water splitting have been reported, including transition-metal oxides,[9] hydroxides,[10] and nitrides[11] for the OER; and metal chalcogenides,[12] carbides,[13] and phosphides[14] for the HER. However, only a few of these reported catalysts are capable of catalyzing both the HER and OER in the same pH range. In general, active OER catalysts work well in a neutral or basic medium, while most HER catalysts perform better in an acidic medium. Recently, iron-group (*e.g.*, Fe, Co, and Ni) alloys encapsulated in nitrogen-doped carbon have become promising candidates for overall water splitting.[15] This is because the close contact between the metal species and the N-doped carbon will induce synergistic electronic coupling effects and directly enrich the active sites.[15,16] Besides, the adsorption energy can be readily tuned by alloying of iron group metals where the lattice spacing and the bond energy can be altered by the composition.[17] The electrocatalytic properties can be further improved by eliminating the grain boundaries in the materials to enhance the electrical transport.[18] Compared with polycrystalline, a single-crystalline structure has higher electrical conductivity and a more robust structure for water splitting, exhibiting better catalytic activity and stability.[19,20] To this end, it is expected that the design and production of single-crystalline iron group alloys encapsulated in nitrogen-doped carbon will enable more efficient overall water splitting.

[a] Department of Chemistry and Biochemistry, University of California Santa Barbara, Santa Barbara, California 93106, USA

[b] Department of Chemistry, University of California Riverside, Riverside, California 92521, USA. E-mail: yadong.yin@ucr.edu

[c] Surface Technology Division, Korea Institute of Materials Science, Changwon 51508, Republic of Korea

[d] Advanced Materials Engineering, Korea University of Science and Technology (UST), Yuseong-gu, Daejeon 34113, Republic of Korea

[e] Hydrogen Laboratory, Research Institute for New and Renewable Energy, Korea Institute of Energy Research, Yuseong, Daejeon 34129, Republic of Korea

[f] Department of Chemical and Environmental Engineering, University of California Riverside, Riverside, California 92521, USA. E-mail: myung@engr.ucr.edu

† Electronic supplementary information (ESI) available. See DOI: 10.1039/d0qm00126k

Herein, we report a simple and efficient method to synthesize single-crystalline cobalt–iron (CoFe) alloy nanoparticles encapsulated in N-doped carbon nanotubes (CoFe@N–C). Upon calcination, the single-crystalline CoFe alloy particles catalyze the formation of N-doped carbon nanotubes (CNTs), which provide high electrical conductivity, inhibit the oxidation of the metal alloy, and result in high catalytic activity and excellent stability towards overall water splitting.

Experimental section

Material synthesis

The synthesis of the single-crystalline CoFe alloy encapsulated in N-doped carbon nanotubes (CoFe@N–C) was based on a simple heat-treatment process. In general, $Co(NO_3)_2$ (0.17 mmol), $Fe(NO_3)_3$ (0.17 mmol), and urea (12 mmol) were dissolved in deionized water (10 mL). After stirring for 2 h and sonicating for 1 h, the resulting solution was dried in a vacuum at 70 °C for 12 h. The obtained precipitate was heat-treated in an N_2 atmosphere at 600, 700, or 800 °C for 2 h with a ramp rate of 5 °C min^{-1}. In addition, the content of urea was adjusted to further elucidate the catalytic activity of the electrocatalyst.

Material characterization

The microstructures of the synthesized products were observed by scanning electron microscopy (SEM, XL30-FEG) and transmission electron microscopy (TEM, JEM-2100F, JEOL). The crystal phases of the samples were analyzed by X-ray diffraction (Bruker SMART APEX2). The chemical composition was investigated by X-ray photoelectron spectroscopy (XPS, AXIS ULTRA). The Raman spectra were excited by a 532 nm laser (Dilor Laser Raman) with a 50 L lens. The concentration of metal ions was measured with an Inductively Coupled Plasma Optical-Emission Spectrometer (ICP-OES) iCAP 6000 Series.

Electrochemical measurements

All electroanalytical methods (i.e., Cyclic Voltammetry (CV), Linear Sweep Voltammetry (LSV), Chronoamperometry (CA) and Electrochemical Impedance Spectroscopy (EIS)) were carried out in a three-electrode cell controlled by a Princeton VersaSTAT 4 electrochemical workstation. 1 M KOH solution was used as the electrolyte. A graphite rod and saturated calomel electrode (SCE) were used as the counter electrode and reference electrode, respectively. The catalyst loading was 0.5 g cm^{-2}. CV curves were recorded at scan rates of 10, 20, 50, and 100 mV s^{-1}. LSV curves were obtained at a scan rate of 5 mV s^{-1}. CA was performed under a constant potential for 20 h. EIS was conducted over a frequency range from 0.01 to 10^5 Hz at the open-circuit potential with an AC voltage amplitude of 10 mV. All the measured potentials versus SCE were converted to a reversible hydrogen electrode (RHE) scale according to the Nernst equation ($E_{RHE} = E_{SCE} + 0.0591pH + 0.242$). The electrochemical measurements in this work were conducted without iR-correction.

Results and discussion

The fabrication process of the CoFe@N–C catalysts is illustrated in Fig. 1a. After solvent evaporation, Co^{2+} and Fe^{3+} ions were uniformly dispersed in urea. Upon heat-treatment, urea was converted into nitrogen-doped carbon, while metal ions were reduced in situ to form an alloy, and then catalyzed to form carbon nanotubes.[21,22] Fig. 1b shows a TEM image of typical CoFe@N–C, from which it was apparent that the metal nanoparticles were encapsulated within the carbon layer or at the ends of the carbon nanotubes. The XRD pattern identified that the samples contained a high-purity body-centered cubic (bcc) CoFe alloy phase (JCPDS No. 49–1567) (Fig. 1c). However, no diffraction peak of carbon was detected, which might be attributed to the high crystallinity of the alloy and the low crystallinity of carbon. This will be further discussed in this work based on the HR-TEM and XPS results.

TEM was conducted to investigate the morphological characteristics of the CoFe alloy encapsulated in N-doped carbon nanotubes. Representative TEM images (Fig. 2a) of CoFe@N–C showed that parts of the metal nanoparticles were encapsulated by carbon to form a core–shell structure. There were also some metal nanoparticles distributed at the tip of the CNTs, which was consistent with the literature.[21,23] The magnified TEM image shown in Fig. 2b revealed metal nanoparticles with a size of ∼100 nm and CNTs with a thickness of ∼8 nm. Of note, the metal nanoparticles showed a single-crystalline feature, as evidenced by the high-resolution transmission electron microscopy (HR-TEM) image (Fig. 2c). HR-TEM showed that the interplanar spacing was 0.2 nm, corresponding to a body-centered cubic CoFe alloy (110),[24,25] which was further confirmed by the selected area electron diffraction (SAED) pattern (inset of Fig. 2c). Moreover, the HR-TEM image of the carbon layer showed a lattice fringe of 0.34 nm corresponding to the
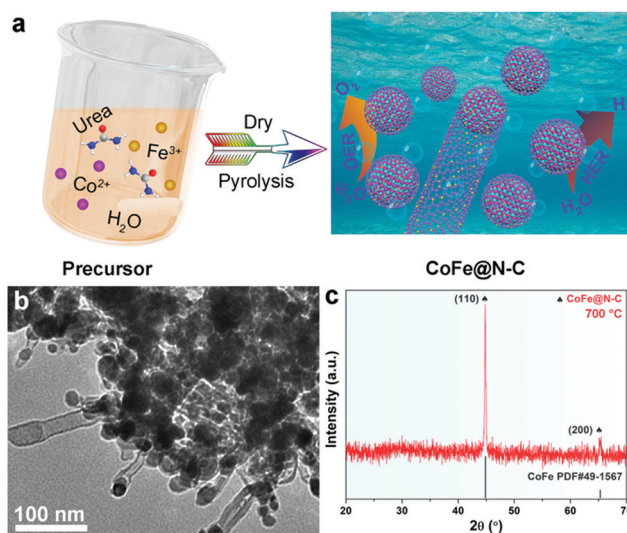

Fig. 1 (a) Schematic illustration of the synthetic procedure of the CoFe@N–C catalysts. (b) TEM image and (c) XRD pattern of the as-synthesized CoFe@N–C.
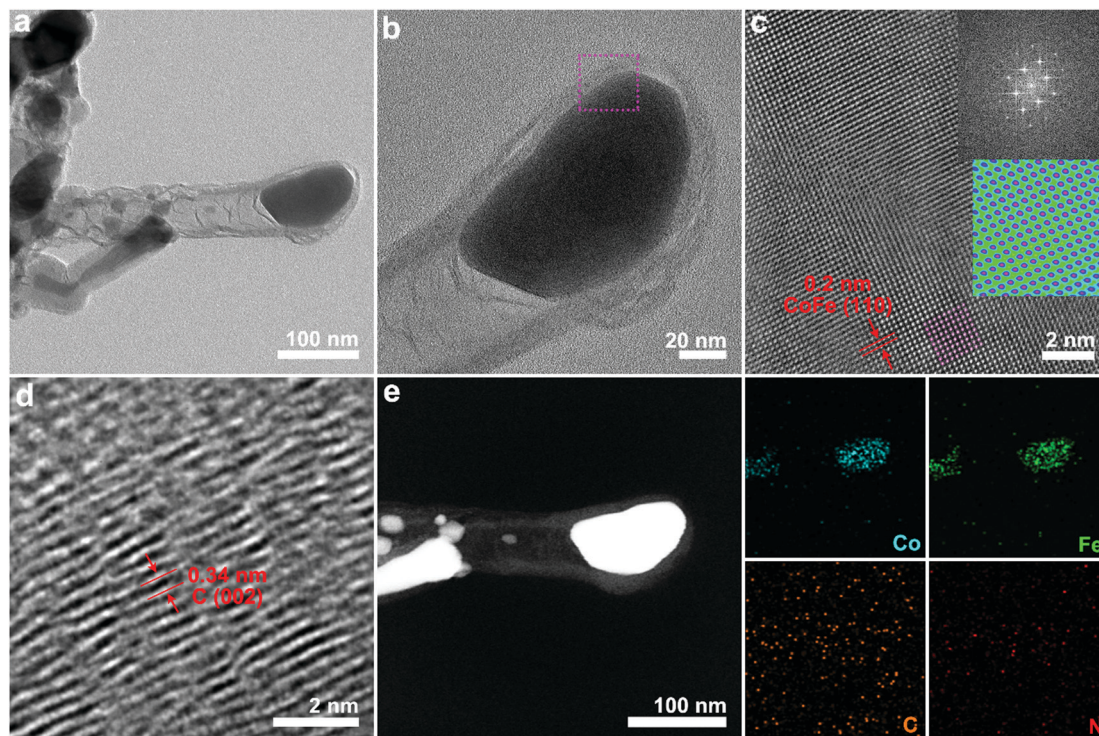
Fig. 2 Characterization of the CoFe@N−C catalysts. (a and b) TEM, (c and d) HR-TEM, and (e) elemental mapping images of as-synthesized CoFe@N−C calcined at 700 °C.

(002) plane of graphite carbon (Fig. 2d). The energy dispersive X-ray (EDX) elemental mapping image (Fig. 2e) of CoFe@N−C presented a homogenous distribution of Co and Fe elements in the metal nanoparticle region. Additionally, the sample contained abundant N element, which was uniformly distributed throughout the carbon nanotube region. The close contact

between the single-crystalline CoFe alloy and the N-doped carbon nanotubes facilitated the overall water splitting.[15,16]

XPS was performed to further analyze the elemental information of the samples. Fig. 3a shows that the atomic percentages of Co, Fe, N, C and O in CoFe@N−C were 15.1%, 15.7%, 1.6%, 36.3%, and 31.3%, respectively. The Co/Fe atom ratio was

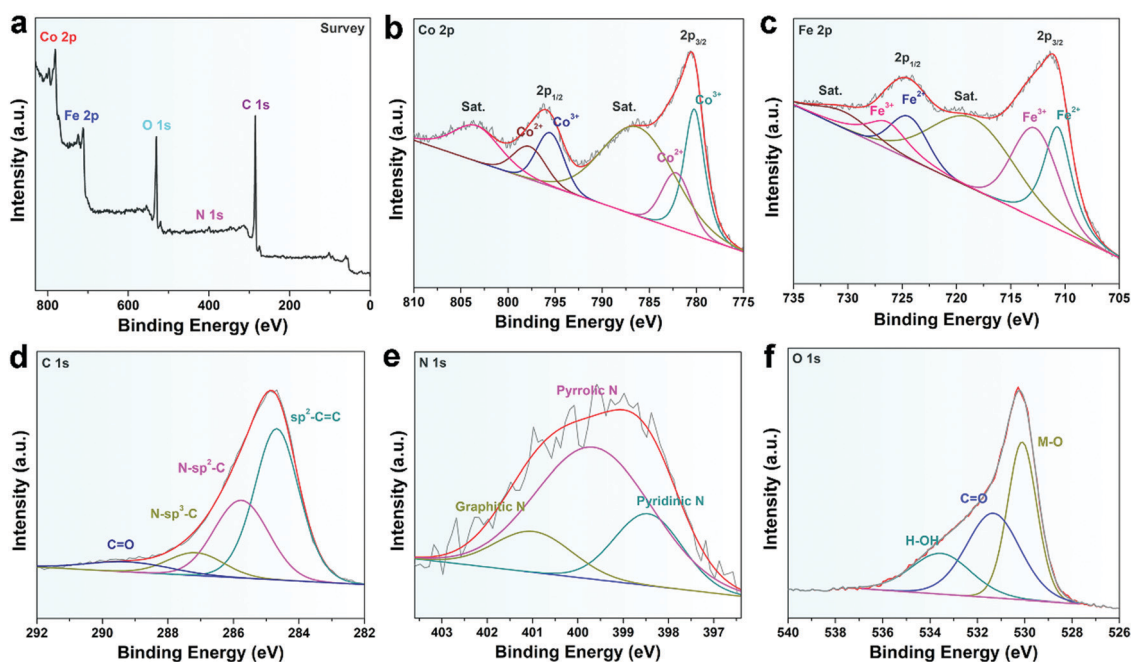Fig. 3 XPS spectra of (a) survey, (b) Co 2p, (c) Fe 2p, (d) C 1s, (e) N 1s, and (f) O 1s of the CoFe@N−C catalysts.

This journal is © The Royal Society of Chemistry and the Chinese Chemical Society 2020

Mater. Chem. Front., 2020, 4, 2307−2313 | 2309

approximately 1, which was consistent with the results of ICP measurements (Table S1, ESI†) and was close to the stoichiometric CoFe alloy. The carbon content in CoFe@N–C calcined at 600 °C and 800 °C was detected to be 35.4% and 37.4%, respectively. As shown in Fig. 3b, the XPS of Co 2p was deconvoluted into Co^{3+} doublet peaks (780.2 and 795.7 eV), Co^{2+} doublet peaks (782.2 and 798.0 eV) and two satellite peaks (786.8 and 803.9 eV).[25,26] Similarly, the XPS of Fe 2p (Fig. 3c) displays Fe^{2+} doublet peaks (710.6 and 724.6 eV), Fe^{3+} doublet peaks (713.0 and 726.8 eV) and two satellite peaks (719.1 and 731.0 eV).[25,26] High valence metals were mainly due to partial electron transfer of surface metal–oxygen species. In the high-resolution XPS C 1s spectrum (Fig. 3d), the four peaks at about 284.6 eV, 285.8 eV, 287.3 eV, and 289.4 eV were attributable to sp^2–C=C, N–sp^2–C, N–sp^3–C, and C=O groups, respectively, which illustrated N-doped carbon. Furthermore, the N 1s XPS spectrum exhibited three peaks derived from pyridinic N (398.5 eV), pyrrolic N (399.7 eV), and graphitic N (401.1 eV) (Fig. 3e), suggesting the abundance of N in the CoFe@N–C samples. The O 1s spectrum (Fig. 3f) showed three peaks at 530.1, 531.4, and 533.6 eV corresponding to the lattice oxygen in O–metal, C=O groups, and surface-adsorbed water molecules, respectively.[27]

To obtain satisfactory CoFe@N–C with well-controlled crystallinity and composites for high electrocatalytic performance, several conditions including the calcination temperature and urea loading were investigated and optimized. It can be seen from Fig. 4 that as the temperature increased the average size of the alloy particles (Fig. 4a and b), as well as the crystallinity (Fig. 4e), increased. To some extent, large-sized metal particles would reduce the density of active sites, thereby reducing the

catalytic activity. Meanwhile, the content of CNTs seemed to be increasing (Fig. 4a and b), which improved the electrical conductivity of the matrix material. Therefore, there is a suitable calcination temperature to balance the activity and electrical conductivity of the catalyst. The intensity of I_D/I_G for CoFe@N–C calcined at 700 °C reached 1.03 (Fig. 4f), indicating that structural defects were introduced due to the N-doping.[28] More importantly, the sample synthesized without the addition of urea was a mixed phase of Co_3Fe_5 and $CoFe_2O_4$ (Fig. 4d and e), and the size of the particles was very large (Fig. 4c). This was attributed to the fact that without the protection of the carbon layer, the surface of the alloy particles was more susceptible to oxidation and thus the particles were prone to overgrowth.

Fig. 5a and b show the linear sweep voltammetry (LSV) curves for the OER and corresponding Tafel slope of CoFe calcined at 700 °C without urea and CoFe@N–C calcined at different temperatures in 1 M KOH. It was found that the CoFe@N–C catalysts calcined at different temperatures presented similar catalytic activity, but CoFe@N–C calcined at 700 °C exhibited the best OER activity with an overpotential of 292 mV at 10 mA cm^{-2} (Fig. 5a). This was further confirmed by its lowest Tafel slope (64 mV dec^{-1}) (Fig. 5b). CoFe calcined at 700 °C without urea showed a relatively low OER activity, probably because metal alloy nanoparticles without the protection of the N-doped carbon layer were easily oxidized during electrochemical testing, and the overall conductivity of the catalyst was relatively poor. EIS of CoFe particles without the N-doped carbon coating shows higher charge-transfer resistance (R_{ct}) with semi-infinite Warburg impedance (Z_w) at low frequency, whereas the N-doped carbon-coated CoFe
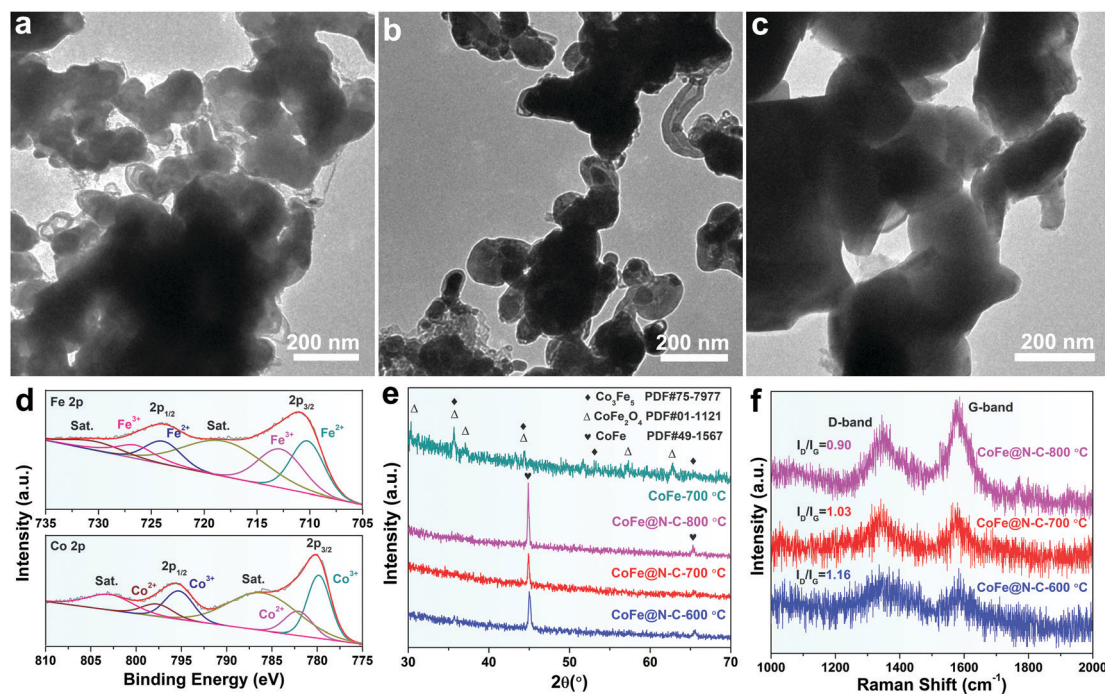

Fig. 4 (a and b) TEM images of CoFe@N–C calcined at (a) 600 °C and (b) 800 °C. (c and d) TEM images (c) and XPS spectra (d) of CoFe calcined at 700 °C without urea. (e and f) Corresponding XRD patterns (e) and Raman spectra (f) of different samples.
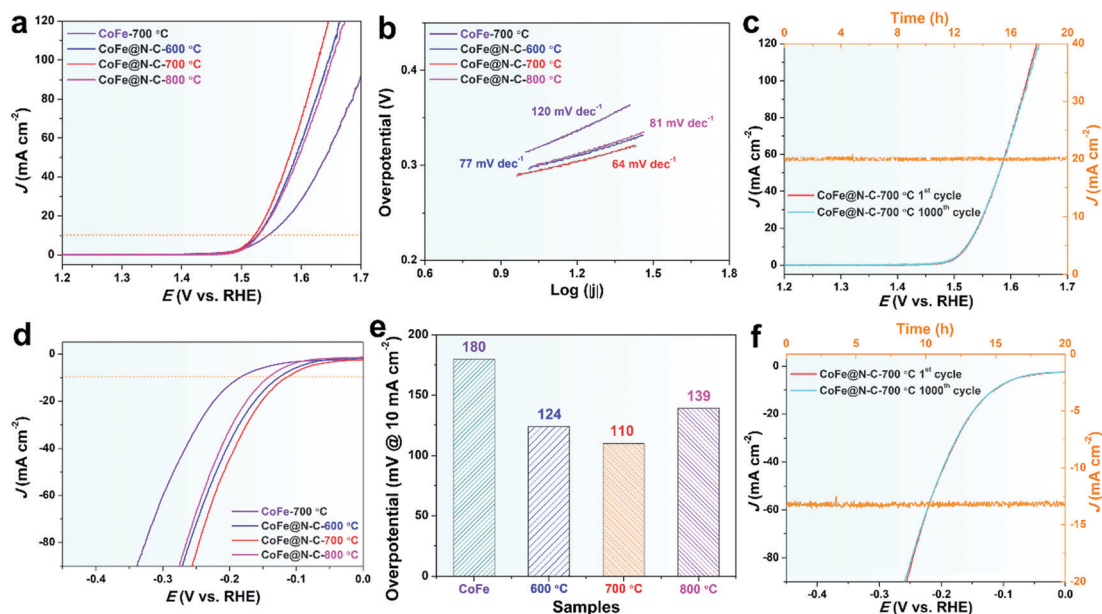
Fig. 5 (a) OER polarization curves and (b) corresponding Tafel slope of CoFe calcined at 700 °C without urea and CoFe@N−C calcined at different temperatures. (c) OER stability test of CoFe@N−C calcined at 700 °C. (d and e) HER polarization curves (d) and corresponding overpotential (e) at 10 mA cm^{-2} of CoFe calcined at 700 °C without urea and CoFe@N−C calcined at different temperatures. (f) HER stability test of CoFe@N−C calcined at 700 °C. All tests were performed in 1 M KOH.

particles show lower charge-transfer resistance (R_{ct}) without Warburg impedance. The difference may be attributed to the ability of N-doped carbon to enhance electron transfer. The electrochemically active surface (ECSA) of various samples was determined from the double-layer capacitance (C_{dl}) (Fig. S1, ESI†) where the CoFe@C-700 sample displayed the highest C_{dl} (*i.e.*, 8 mF cm^{-2}). In addition to its high OER activity, CoFe@N−C showed very good stability and durability with no observable deviation in the overpotential for the OER after 1000 cycles of CV (100 mV s^{-1}, Fig. 5c) and no decay in the current density over 20 h of applying a constant potential (Fig. 5c).

As mentioned, an ideal electrocatalyst is expected to reduce the activation energy of both the OER and HER,[3] especially in the same pH range.[29] In this regard, the HER activity of CoFe@N−C in 1 M KOH was explored. Interestingly, CoFe@N−C

calcined at 700 °C displayed good HER activity with an overpotential of 110 mV at 10 mA cm^{-2} in 1 M KOH (Fig. 5d and e), which was much lower than the overpotential of CoFe calcined at 700 °C (180 mV). This further demonstrated the important role of the N-doped carbon layer. It is worth noting that the CoFe@N−C catalysts also showed superb HER stability in alkaline media. As observed in Fig. 5f, after 1000 CV cycles (100 mV s^{-1}), the overpotential of CoFe@N−C calcined at 700 °C was practically unchanged. At the same time, there was no obvious decrease in the current density of CoFe@N−C after the constant potential test for 20 h.

All the above results indicated that the CoFe@N−C catalyst was indeed a highly efficient and durable electrocatalyst towards overall water splitting in alkaline media, which makes it a promising material as one of the advanced-level reported electrocatalysts for overall water splitting, as summarized in Table 1, and it shows potential for large-scale application due to its simple and cost-effective preparation methods. The excellent catalytic activity and superior stability of CoFe@N−C were mainly due to the synergetic effect of highly conductive carbon, abundant nitrogen doping, and the single-crystalline feature.

Conclusion

In summary, a simple and cost-effective heat-treatment method was developed to fabricate single-crystalline CoFe alloy particles encapsulated in N-doped carbon nanotubes (CoFe@N−C). The resulting electrocatalyst was stable, bifunctional, and highly efficient toward overall water splitting, exhibiting a low overpotential of 292 mV and 110 mV (at 10 mA cm^{-2}) to drive the OER and HER, respectively.

Table 1 Electrocatalytic performances toward overall water splitting of CoFe@N−C and reported non-noble metal-based catalysts in 1 M KOH

Electrocatalysts	Loading (mg cm^{-2})	OER η (mV) @10 mA cm^{-2}	HER η (mV) @10 mA cm^{-2}	Ref.
MoP	0.3	265	114	30
Ni–Co–P	N/A	270	107	29
FeNi/NPC	0.6	230	200	15
P-Co$_3$O$_4$	0.4	280	120	31
CoFe@N−C	0.5	292	110	This work
Co(S$_{0.47}$Se$_{0.53}$)$_2$	1.0	290	128	32
S:CoP	0.4–0.5	∼300	109	33
Co/NBC-900	1.2–1.8	302	117	34
CoP/NCNHP	N/A	310	115	35
CP/CTs/Co–S	N/A	306	190	36
δ-MnO$_2$	0.35	320	197	37
Co$_9$S$_8$@NOSC	0.28	340	320	38

Conflicts of interest

There are no conflicts to declare.

Acknowledgements

References

1 H. T. Wang, H. W. Lee, Y. Deng, Z. Y. Lu, P. C. Hsu, Y. Y. Liu, D. C. Lin and Y. Cui, Bifunctional non-noble metal oxide nanoparticle electrocatalysts through lithium-induced conversion for overall water splitting, *Nat. Commun.*, 2015, **6**, 7261.

2 H. Y. Li, S. M. Chen, Y. Zhang, Q. H. Zhang, X. F. Jia, Q. Zhang, L. Gu, X. M. Sun, L. Song and X. Wang, Systematic design of superaerophobic nanotube-array electrode comprised of transition-metal sulfides for overall water splitting, *Nat. Commun.*, 2018, **9**, 2452.

3 Y. Y. Liang, Y. G. Li, H. L. Wang and H. J. Dai, Strongly Coupled Inorganic/Nanocarbon Hybrid Materials for Advanced Electrocatalysis, *J. Am. Chem. Soc.*, 2013, **135**, 2013–2036.

4 D. Y. Chung, S. W. Jun, G. Yoon, H. Kim, J. M. Yoo, K. S. Lee, T. Kim, H. Shin, A. K. Sinha, S. G. Kwon, K. Kang, T. Hyeon and Y. E. Sung, Large-scale synthesis of carbon-shell-coated FeP nanoparticles for robust hydrogen evolution reaction electrocatalyst, *J. Am. Chem. Soc.*, 2017, **139**, 6669–6674.

5 X. J. Zeng, J. L. Shui, X. F. Liu, Q. T. Liu, Y. C. Li, J. X. Shang, L. R. Zheng and R. H. Yu, Single-Atom to Single-Atom Grafting of Pt_1 onto $Fe-N_4$ Center: $Pt_1@Fe–N–C$ Multifunctional Electrocatalyst with Significantly Enhanced Properties, *Adv. Energy Mater.*, 2018, **8**, 1701345.

6 P. T. Wang, X. Zhang, J. Zhang, S. Wan, S. J. Guo, G. Lu, J. L. Yao and X. Q. Huang, Precise tuning in platinum-nickel/nickel sulfide interface nanowires for synergistic hydrogen evolution catalysis, *Nat. Commun.*, 2017, **8**, 14580.

7 Z. H. Pu, I. S. Amiinu, Z. K. Kou, W. Q. Li and S. C. Mu, RuP_2-Based Catalysts with Platinum-like Activity and Higher Durability for the Hydrogen Evolution Reaction at All pH Values, *Angew. Chem.*, 2017, **129**, 11717–11722.

8 I. Roger, M. A. Shipman and M. D. Symes, Earth-abundant catalysts for electrochemical and photoelectrochemical water splitting, *Nat. Rev. Chem.*, 2017, **1**, 0003.

9 Z. Chen, B. Zhao, Y.-C. He, H.-R. Wen, X.-Z. Fu, R. Sun and C.-P. Wong, $NiCo_2O_4$ nanoframes with a nanosheet surface as efficient electrocatalysts for the oxygen evolution reaction, *Mater. Chem. Front.*, 2018, **2**, 1155–1164.

10 S. H. Ye, Z. X. Shi, J. X. Feng, Y. X. Tong and G. R. Li, Activating CoOOH porous nanosheet arrays by partial iron substitution for efficient oxygen evolution reaction, *Angew. Chem., Int. Ed.*, 2018, **57**, 2672–2676.

11 K. Xu, P. Z. Chen, X. L. Li, Y. Tong, H. Ding, X. J. Wu, W. S. Chu, Z. M. Peng, C. Z. Wu and Y. Xie, Metallic nickel nitride nanosheets realizing enhanced electrochemical water oxidation, *J. Am. Chem. Soc.*, 2015, **137**, 4119–4125.

12 M. A. Lukowski, A. S. Daniel, F. Meng, A. Forticaux, L. Li and S. Jin, Enhanced Hydrogen Evolution Catalysis from Chemically Exfoliated Metallic MoS_2 Nanosheets, *J. Am. Chem. Soc.*, 2013, **135**, 10274–10277.

13 Y. Zheng, Y. Jiao, Y. H. Zhu, L. H. Li, Y. Han, Y. Chen, A. J. Du, M. Jaroniec and S. Z. Qiao, Hydrogen evolution by a metal-free electrocatalyst, *Nat. Commun.*, 2014, **5**, 3783.

14 S. Jeoung, B. Seo, J. M. Hwang, S. H. Joo and H. R. Moon, Direct conversion of coordination compounds into Ni_2P nanoparticles entrapped in 3D mesoporous graphene for an efficient hydrogen evolution reaction, *Mater. Chem. Front.*, 2017, **1**, 973–978.

15 H. X. Zhong, J. Wang, Q. Zhang, F. L. Meng, D. Bao, T. Liu, X. Y. Yang, Z. W. Chang, J. M. Yan and X. B. Zhang, In Situ Coupling FeM (M = Ni, Co) with Nitrogen-Doped Porous Carbon toward Highly Efficient Trifunctional Electrocatalyst for Overall Water Splitting and Rechargeable Zn-Air Battery, *Adv. Sustainable Syst.*, 2017, **1**, 1700020.

16 Z. Y. Wu, X. X. Xu, B. C. Hu, H. W. Liang, Y. Lin, L. F. Chen and S. H. Yu, Iron carbide nanoparticles encapsulated in mesoporous Fe-N-doped carbon nanofibers for efficient electrocatalysis, *Angew. Chem., Int. Ed.*, 2015, **54**, 8179.

17 Y. Yang, Z. Y. Lun, G. L. Xia, F. C. Zheng, M. N. He and Q. W. Chen, Non-precious alloy encapsulated in nitrogen-doped graphene layers derived from MOFs as an active and durable hydrogen evolution reaction catalyst, *Energy Environ. Sci.*, 2015, **8**, 3563–3571.

18 S. Y. Nong, W. J. Dong, J. W. Yin, B. W. Dong, Y. Lu, X. T. Yuan, X. Wang, K. J. Bu, M. Y. Chen, S. D. Jiang, L. M. Liu, M. L. Sui and F. Q. Huang, Well-Dispersed Ruthenium in Mesoporous Crystal TiO_2 as an Advanced Electrocatalyst for Hydrogen Evolution Reaction, *J. Am. Chem. Soc.*, 2018, **140**, 5719–5727.

19 C. W. Tung, Y. Y. Hsu, Y. P. Shen, Y. X. Zheng, T. S. Chan, H. S. Sheu, Y. C. Cheng and H. M. Chen, Reversible adapting layer produces robust single-crystal electrocatalyst for oxygen evolution, *Nat. Commun.*, 2015, **6**, 8106.

20 Y. Kuang, Y. Zhang, Z. Cai, G. Feng, Y. Y. Jiang, C. H. Jin, J. Luo and X. M. Sun, Single-crystalline dendritic bimetallic and multimetallic nanocubes, *Chem. Sci.*, 2015, **6**, 7122–7129.

21 S. Esconjauregui, C. M. Whelan and K. Maex, The reasons why metals catalyze the nucleation and growth of carbon nanotubes and other carbon nanomorphologies, *Carbon*, 2009, **47**, 659–669.

22 W. Q. Deng, X. Xu and W. A. Goddard, A two-stage mechanism of bimetallic catalyzed growth of single-walled carbon nanotubes, *Nano Lett.*, 2004, **4**, 2331–2335.

23 J. A. Rodríguez-Manzo, M. Terrones, H. Terrones, H. W. Kroto, L. T. Sun and F. Banhart, *In situ* nucleation of carbon nanotubes by the injection of carbon atoms into metal particles, *Nat. Nanotechnol.*, 2007, **2**, 307–311.

2312 | *Mater. Chem. Front.*, 2020, **4**, 2307–2313

This journal is © The Royal Society of Chemistry and the Chinese Chemical Society 2020

24 Y. Liu, F. Li, H. D. Yang, J. Li, P. Ma, Y. Zhu and J. T. Ma, Two-Step Synthesis of Cobalt Iron Alloy Nanoparticles Embedded in Nitrogen-Doped Carbon Nanosheets/Carbon Nanotubes for the Oxygen Evolution Reaction, *ChemSusChem*, 2018, **11**, 2358–2366.

25 F. H. Kong, K. F. Chen, S. Y. Song and D. F. Xue, Metal organic framework derived CoFe@N-doped carbon/reduced graphene sheets for enhanced oxygen evolution reaction, *Inorg. Chem. Front.*, 2018, **5**, 1962–1966.

26 X. J. Ma, H. Chai, Y. L. Cao, J. Y. Xu, Y. C. Wang, H. Dong, D. Z. Jia and W. Y. Zhou, An effective bifunctional electrocatalysts: Controlled growth of CoFe alloy nanoparticles supported on N-doped carbon nanotubes, *J. Colloid Interface Sci.*, 2018, **514**, 656–663.

27 H. Ding, Y. Ji, J. S. Wei, Q. Y. Gao, Z. Y. Zhou and H. M. Xiong, Facile synthesis of red-emitting carbon dots from pulp-free lemon juice for bioimaging, *J. Mater. Chem. B*, 2017, **5**, 5272–5277.

28 S. Y. Wang, L. P. Zhang, Z. H. Xia, A. Roy, D. W. Chang, J. B. Baek and L. M. Dai, BCN graphene as efficient metal-free electrocatalyst for the oxygen reduction reaction, *Angew. Chem., Int. Ed.*, 2012, **51**, 4209–4212.

29 E. L. Hu, Y. F. Feng, J. W. Nai, D. Zhao, Y. Hu and X. W. Lou, Construction of hierarchical Ni-Co-P hollow nanobricks with oriented nanosheets for efficient overall water splitting, *Energy Environ. Sci.*, 2018, **11**, 872–880.

30 Y. Y. Jiang, Y. Z. Lu, J. Y. Lin, X. Wang and Z. X. Shen, A Hierarchical MoP Nanoflake Array Supported on Ni Foam: A Bifunctional Electrocatalyst for Overall Water Splitting, *Small Methods*, 2018, **2**, 1700369.

31 Z. H. Xiao, Y. Wang, Y. C. Huang, Z. X. Wei, C. L. Dong, J. M. Ma, S. H. Shen, Y. F. Li and S. Y. Wang, Filling the oxygen vacancies in Co_3O_4 with phosphorus: an ultra-efficient electrocatalyst for overall water splitting, *Energy Environ. Sci.*, 2017, **10**, 2563–2569.

32 L. Fang, W. X. Li, Y. X. Guan, Y. Y. Feng, H. J. Zhang, S. L. Wang and Y. Wang, Tuning Unique Peapod-Like $Co(S_xSe_{1−x})_2$ Nanoparticles for Efficient Overall Water Splitting, *Adv. Funct. Mater.*, 2017, **27**, 1701008.

33 M. A. R. Anjum, M. S. Okyay, M. Kim, M. H. Lee, N. Park and J. S. Lee, Bifunctional sulfur-doped cobalt phosphide electrocatalyst outperforms all-noble-metal electrocatalysts in alkaline electrolyzer for overall water splitting, *Nano Energy*, 2018, **53**, 286–295.

34 M. R. Liu, Q. L. Hong, Q. H. Li, Y. H. Du, H. X. Zhang, S. M. Chen, T. H. Zhou and J. Zhang, Cobalt Boron Imidazolate Framework Derived Cobalt Nanoparticles Encapsulated in B/N Codoped Nanocarbon as Efficient Bifunctional Electrocatalysts for Overall Water Splitting, *Adv. Funct. Mater.*, 2018, **28**, 1801136.

35 Y. Pan, K. A. Sun, S. J. Liu, X. Cao, K. L. Wu, W. C. Cheong, Z. Chen, Y. Wang, Y. Li, Y. Q. Liu, D. S. Wang, Q. Peng, C. Chen and Y. D. Li, Core-shell ZIF-8@ZIF-67-derived CoP nanoparticle-embedded N-doped carbon nanotube hollow polyhedron for efficient overall water splitting, *J. Am. Chem. Soc.*, 2018, **140**, 2610–2618.

36 J. Wang, H. X. Zhong, Z. L. Wang, F. L. Meng and X. B. Zhang, Integrated three-dimensional carbon paper/carbon tubes/cobalt-sulfide sheets as an efficient electrode for overall water splitting, *ACS Nano*, 2016, **10**, 2342–2348.

37 Y. X. Zhao, C. Chang, F. Teng, Y. F. Zhao, G. B. Chen, R. Shi, G. I. N. Waterhouse, W. F. Huang and T. R. Zhang, Defect-Engineered Ultrathin δ-MnO₂ Nanosheet Arrays as Bifunctional Electrodes for Efficient Overall Water Splitting, *Adv. Energy Mater.*, 2017, **18**, 1700005.

38 S. C. Huang, Y. Y. Meng, S. M. He, A. Goswami, Q. L. Wu, J. H. Li, S. F. Tong, T. Asefa and M. M. Wu, N-, O-, and S-Tridoped Carbon-Encapsulated Co_9S_8 Nanomaterials: Efficient Bifunctional Electrocatalysts for Overall Water Splitting, *Adv. Funct. Mater.*, 2017, **27**, 1606585.